Is Alaska's Yukon–Kuskokwim Delta Greening or Browning? Resolving Mixed Signals of Tundra Vegetation Dynamics and Drivers in the Maritime Arctic

GERALD V. FROST,[a] UMA S. BHATT,[b] MATTHEW J. MACANDER,[a] AMY S. HENDRICKS,[b] AND M. TORRE JORGENSON[c]

[a] *ABR, Inc.—Environmental Research and Services, Fairbanks, Alaska*
[b] *Geophysical Institute, University of Alaska Fairbanks, Fairbanks, Alaska*
[c] *Alaska Ecoscience, Fairbanks, Alaska*

(Manuscript received 26 October 2020, in final form 23 April 2021)

ABSTRACT: Alaska's Yukon–Kuskokwim Delta (YKD) is among the Arctic's warmest, most biologically productive regions, but regional decline of the normalized difference vegetation index (NDVI) has been a striking feature of spaceborne Advanced High Resolution Radiometer (AVHRR) observations since 1982. This contrast with ''greening'' prevalent elsewhere in the low Arctic raises questions concerning climatic and biophysical drivers of tundra productivity along maritime–continental gradients. We compared NDVI time series from AVHRR, the Moderate Resolution Imaging Spectroradiometer (MODIS), and Landsat for 2000–19 and identified trend drivers with reference to sea ice and climate datasets, ecosystem and disturbance mapping, field measurements of vegetation, and knowledge exchange with YKD elders. All time series showed increasing maximum NDVI; however, whereas MODIS and Landsat trends were very similar, AVHRR-observed trends were weaker and had dissimilar spatial patterns. The AVHRR and MODIS records for time-integrated NDVI were dramatically different; AVHRR indicated weak declines, whereas MODIS indicated strong increases throughout the YKD. Disagreement largely arose from observations during shoulder seasons, when there is partial snow cover and very high cloud frequency. Nonetheless, both records shared strong correlations with spring sea ice extent and summer warmth. Multiple lines of evidence indicate that, despite frequent disturbances and high interannual variability in spring sea ice and summer warmth, tundra productivity is increasing on the YKD. Although climatic drivers of tundra productivity were similar to more continental parts of the Arctic, our intercomparison highlights sources of uncertainty in maritime areas like the YKD that currently, or soon will, challenge historical concepts of ''what is Arctic.''

KEYWORDS: Arctic; Sea ice; Vegetation–atmosphere interactions; Trends; Ecosystem effects

1. Introduction

Western Alaska's Yukon–Kuskokwim Delta (YKD) is one of the most biologically productive regions of the circumpolar Arctic and home to ~30 000 Yup'ik people, one of the largest subsistence-based indigenous populations in North America (Rearden and Fienup-Riordan 2014). The YKD is renowned as a globally significant breeding area for migratory waterbirds (Spencer et al. 1951; Gill and Handel 1990), and subsistence resources obtained from YKD ecosystems are vital to Yup'ik economy and culture (Klein 1966; Fienup-Riordan 1999; Herman-Mercer et al. 2019). The impacts of climate change to YKD ecosystems and the services they provide are therefore of great societal concern within and beyond the region. Many of the rapid changes to marine and terrestrial ecosystems reported from the panarctic have also been widely reported by YKD residents and land managers, including sea ice decline (Grebmeier et al. 2006), permafrost thaw (Whitley et al. 2018; Michaelides et al. 2019), changing tundra productivity (Bhatt et al. 2010; Bieniek et al. 2015), tundra shrub expansion (Myers-Smith et al. 2011), and increased coastal flooding and erosion (Vermaire et al. 2013). These processes have already driven changes to the abundance and management of marine and terrestrial resources [e.g., fisheries and moose (*Alces alces*)] (Mueter and Litzow 2008; Perry 2010), and even prompted the relocation of villages (e.g., Newtok). Yet, current understanding of Arctic environmental change is spatially biased toward colder, more continental regions, while maritime regions such as the YKD remain little studied.

The dynamic coastal and riverine processes that underpin the YKD's biological productivity also increase the region's vulnerability to warming-induced environmental changes, including sea level rise, delayed formation of sea ice, and increased storm surge and saltwater intrusion (Jorgenson and Ely 2001; Atkinson 2005; Kirwan et al. 2010; Terenzi et al. 2014). Projections of global eustatic sea level rise for the twenty-first century range from 0.3 to 1 m (Pachauri et al. 2014) and have urgent implications for the YKD because of the region's very low elevation. In addition, inland areas of the YKD support ice-rich permafrost, but ground temperatures are near the freezing point (Jorgenson 2000). Thus, owing to the climate regime, proximity to the coast, and low-lying topography, YKD ecosystems are vulnerable to rapid and persistent change following shifts across basic thermal and physical thresholds.

Supplemental information related to this paper is available at the Journals Online website: https://doi.org/10.1175/EI-D-20-0025.s1.

Corresponding author: Gerald V. Frost, jfrost@abrinc.com

Earth Interactions is published jointly by the American Meteorological Society, the American Geophysical Union, and the Association of American Geographers.

DOI: 10.1175/EI-D-20-0025.1

Long-term satellite observations of the normalized difference vegetation index (NDVI)—a spectral metric of vegetation productivity (Tucker et al. 1979)—have indicated widespread tundra "greening" across most of the Arctic since 1982 (Myneni et al. 1997; Jia et al. 2003; Bhatt et al. 2010; Park et al. 2016), although these increases have moderated in recent years (Bhatt et al. 2013; Bieniek et al. 2015; Bhatt et al. 2017). Trends evident on the YKD in the Global Inventory Modeling and Mapping Studies 3g, version 1.2 (GIMMS), dataset, collected by the Advanced Very High Resolution Radiometer (AVHRR) instrument aboard polar-orbiting satellites, are notably different when compared with prevailing trends in the circumpolar low Arctic. While the early part of the record was consistent with prevalent circumpolar greening trends, NDVI on the YKD has generally declined after 1998. Declines have been especially prominent in spring and early summer, raising questions about linkages to regional climate, changing seasonality, and extreme events (Bokhorst et al. 2009, 2011; Gamon et al. 2013; Bjerke et al. 2014). However, the GIMMS record is affected by inconsistencies in sensor bandpasses, orbital characteristics, and cross-calibration across the many satellites that have contributed to the record (Latifovic et al. 2012; Pinzon and Tucker 2014). Comparisons between GIMMS and datasets from more modern systems, such as the Moderate Resolution Imaging Spectroradiometer (MODIS) and *Landsat-5–8*, have indicated considerable disagreement in other parts of the Arctic (Beck et al. 2011; Guay et al. 2014; Ju and Masek 2016). The 1/12° (~7 km) spatial resolution of GIMMS is also too coarse to resolve landscape-scale patterns and spatial context concerning the biophysical mechanisms that underlie the NDVI trends—in other words, the changes in surface conditions that might be apparent to an observer on the ground. Higher-resolution time series are therefore critical for corroborating regional browning in the GIMMS record, identifying salient climatic drivers, and distinguishing mechanisms that dampen or enhance productivity changes at the landscape scale (Pastick et al. 2019; Piao et al. 2019).

Here we compare 20 years of concurrent NDVI observations (2000–19) collected by AVHRR GIMMS, MODIS, and *Landsat-5–8* over the YKD. We place our findings in context using gridded datasets for climate and sea ice, detailed landscape and disturbance mapping, field data, and observations from YKD elders concerning ecosystem conditions and change during and preceding the satellite record. We sought to answer the following questions:

1) Do the three satellite records agree on NDVI trends in terms of sign, magnitude, and spatiotemporal pattern during 2000–19?
2) What is the relative importance of summer temperature, precipitation, and spring sea ice extent in controlling tundra vegetation productivity on the YKD, and do these relationships clarify which record(s) are most reliable?
3) Do observed plot-scale dynamics (~1994–2016), landscape-scale disturbance records, and testimonials from YKD elders corroborate the satellite record(s)?

2. Study area

The study area included the combined extents of the Yukon Delta National Wildlife Refuge and the YKD ecoregion (Nowacki et al. 2003), totaling 96 178 km^2 (Fig. 1). Vegetation and climate correspond to bioclimatic subzone E of the Circumpolar Arctic Vegetation Map (CAVM Team 2003; Raynolds et al. 2019). The YKD represents one of the southernmost extents of the Arctic tundra biome and a maritime end member of Arctic climate regimes, with comparatively warm winter temperatures, frequent winter thaw and rain-on-snow events, and variable amounts of coastal sea ice.

Differences in landscape history and a strong coastal–inland climate gradient generate high local variability in the structure, productivity, and phenology of YKD vegetation. Although the YKD is best known for its coastal and deltaic wetlands, upland tundra is widespread on eolian deposits that overlie ancient portions of the delta. Uplands and older delta-floodplain deposits support extensive permafrost and are dominated by low-growing tundra. In contrast, modern deltaic deposits lack permafrost and support extensive riparian shrublands that can exceed 5-m height. To distinguish important relationships between NDVI trends and ecosystem properties, we stratified the study area by six physiography classes that partition the topographic, geomorphic, and hydrologic properties that influence ecosystem development and disturbance regime (Table 1). We delineated physiography by adapting the ecological subsections mapping of Jorgenson and Roth (2010).

3. Methods

a. *NDVI datasets*

1) AVHRR GIMMS

GIMMS NDVI data are derived from AVHRR sensors onboard a series of National Oceanic and Atmospheric Administration (NOAA) satellites (*NOAA-7* through *NOAA-19*). The full dataset summarizes the maximum NDVI value observed for 15–16-day compositing periods since July 1981 (Tucker et al. 2005; Pinzon and Tucker 2014). We used approximately 1/12° (~7 km) resolution NDVI data from 2000 to 2019. The GIMMS dataset we analyzed includes revisions to the record after 2017; these revisions incorporated data from the NOAA *MetOp-B* satellite, rather than the *NOAA-19* satellite that introduced artificially low NDVI values after 2017 in earlier versions of GIMMS (J. Pinzon 2020, personal communication).

2) MODIS

To develop time series best suited for comparison with GIMMS, we used the MODIS Nadir Bidirectional Reflectance Distribution Function (BRDF) Adjusted Reflectance product (MCD43A4, version 6) (Schaaf and Wang 2020). This product provides 500-m reflectance data that are adjusted to model reflectance values as if they were collected at nadir. Data are produced daily within 16-day periods using observations from both MODIS *Terra* and *Aqua*. The product is developed using a single observation from each 16-day period for each pixel, with priority given to the central day in each period (i.e., the ninth day) to provide the most representative seasonal information possible. Unlike MODIS NDVI products, MCD43A4 has a temporal frequency of one day, with the 16-day window shifting one day with each new image; thus, MCD43A4 avoids

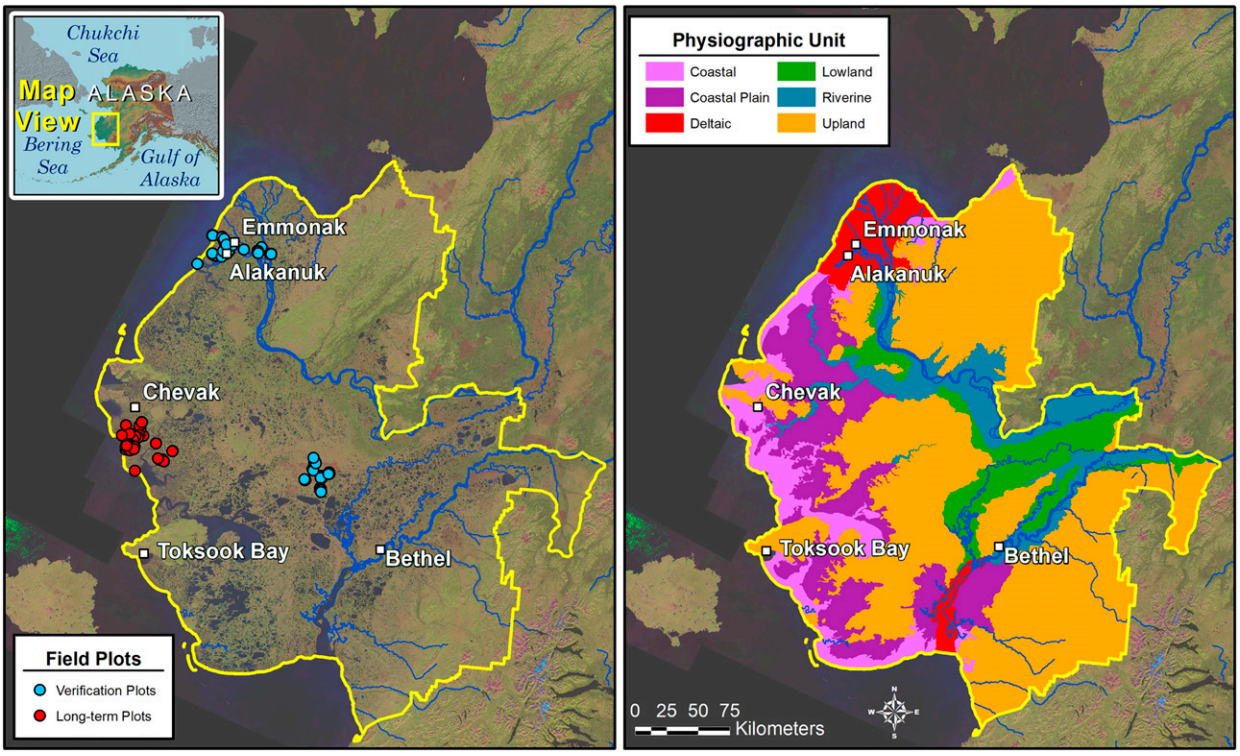

FIG. 1. (left) Overview of study area and field plots, and (right) distribution of physiographic units in the Yukon–Kuskokwim Delta. Physiographic units are adapted from Jorgenson and Roth (2010).

step-change artifacts at the break between composite intervals and NDVI metrics can be calculated for the identical compositing periods as GIMMS. We included results from both full BRDF inversions, and magnitude BRDF inversions when insufficient data are available for the full inversion.

3) LANDSAT

The Landsat archive provides thousands of observations of the YKD at 30-m resolution. We applied all available Collection 1 imagery collected during 2000–19 by the Thematic Mapper (TM), Enhanced Thematic Mapper Plus (ETM+), and Operational

TABLE 1. Description and extent of physiographic units used to stratify the YKD study area.

Physiographic unit	Area (km^2)	Percent of total (%)	Description
Upland	51 553	53.6	Rolling hills and isolated mountains, chiefly of eolian or volcanic origin with mesic soils and high position in local topography
Lowland	7346	7.6	Flat inland areas occupying low position in local topography but not associated with floodplains
Riverine	9385	9.8	Nondeltaic floodplains that experience regular fluvial sedimentation and erosion
Deltaic	5282	5.5	Modern deltas of the Yukon and Kuskokwim Rivers
Coastal plain	14 445	15.0	Flat, low-lying areas near the coast that are not regularly subject to saltwater inundation
Coastal	8167	8.5	Flat, low-lying areas near the coast; generally young surfaces subject to saltwater inundation
Total	96 178	100.0	

Land Imager (OLI) that was processed to surface reflectance and had a geometric root-mean-square error ≤ 30 m. We used the "pixel_qa" band to mask cloud, cloud shadow, snow, and water pixels, and filtered on day-of-year (DOY) to exclude imagery that was not from the midsummer period (1 July–31 August) identified in the NDVI seasonality analysis described below. The three Landsat sensors have different characteristics, so we normalized TM and OLI data to match ETM+ using the surface reflectance NDVI correction factors of Ju and Masek (2016) and Roy et al. (2016), respectively. We evaluated Landsat data density by physiographic unit and determined that valid midsummer observations existed for at least 75% of each unit's extent in all but 4 or 5 years of the 20-yr study period.

b. NDVI seasonality analysis

We used MODIS MCD43A4 to characterize regional gradients in the seasonality of NDVI among tundra ecoregions of southwestern Alaska (Nowacki et al. 2003), and among the six physiographic units within the YKD. For all areas under 200-m elevation, we calculated the overall median NDVI for each DOY to produce climatological normal NDVI curves, with a focus on the midsummer peak of NDVI. We used the curves to determine a DOY range that was wide enough to support trend analysis of Landsat data, while excluding shoulder season dates when NDVI would not be close to its midsummer peak.

NDVI is biased by subpixel water and unusual values are often evident within waterbodies in surface reflectance imagery (Macander 2005). We therefore masked MODIS pixels using the Joint Research Commission global water occurrence layer (Pekel et al. 2016), a 30-m-resolution product that delineates perennial and seasonal waterbodies. To produce a binary water/land classification, we defined water as pixels with ≥ 50% water occurrence. We then aggregated this classification to the 500-m MODIS pixels, and masked MODIS pixels with ≥ 50% water.

c. NDVI trend analysis

Our intercomparison considered three NDVI metrics:

1) Maximum NDVI (MaxNDVI), which is the highest NDVI value observed each year during the period of peak aboveground biomass in midsummer. MaxNDVI represents peak vegetation photosynthetic capacity and is an indicator of aboveground biomass (Shippert et al. 1995; Walker et al. 2003; Raynolds et al. 2012). Thus, MaxNDVI is responsive to disturbance and successional processes, as well as long-term changes such as shrub expansion.
2) Median NDVI (MedianNDVI), which is the median of NDVI values observed during the midsummer seasonal window determined by the seasonality analysis. MedianNDVI is an alternative metric of midsummer productivity that does not rely on extreme (e.g., maximum) values and is less subject to outliers. MedianNDVI also mitigates the tendency of MaxNDVI to be biased high in years with more valid observations, when one of the observations is more likely to be close to the actual date of peak NDVI. This is particularly important for Landsat, which does not collect daily observations and which had high variability in observation frequency over the study period. For AVHRR, we calculated MedianNDVI as the median value of maximum NDVI for the four bimonthly compositing periods during midsummer.
3) Time-integrated NDVI (TI-NDVI), which is the sum of maximum NDVI values >0.05 within the ten bimonthly compositing periods during May–September (i.e., from spring greenup through autumn senescence). TI-NDVI incorporates phenological variations throughout the growing season; therefore, it better represents gross primary production (Tucker and Sellers 1986) and is better correlated with climate variables than MaxNDVI (Bhatt et al. 2010). It was not possible to develop TI-NDVI time series using Landsat because of its much lower observational frequency and excessive data gaps within the 10 bimonthly compositing periods.

For all datasets and metrics, we analyzed per-pixel trends using Theil–Sen robust regression (Sen 1968; Theil 1992) implemented with the "sensSlope" reducer (Clinton 2020) in Google Earth Engine (Gorelick et al. 2017); robust regression is less sensitive to outliers than is standard linear regression. We calculated the slope of regression lines and the statistical p value of trends calculated for each pixel using the nonparametric Mann–Kendall test. To evaluate spatial patterns of trend, we produced maps showing grid cells for which $p < 0.1$. We also summarized observations in the form of time series plots. Last, we evaluated the seasonality of trends by dividing the GIMMS and MODIS MaxNDVI records by compositing period for May–September. To mitigate the effects of waterbodies on NDVI analyses, we applied the binary land/water map described above in two ways. For trend maps, we masked "water" pixels; in the time series and trend seasonality plots, we weighted each pixel value based on its land fraction (100% land is weighted 100%, 75% land is weighted 75%, etc.).

d. Trend drivers

1) CLIMATIC VARIABLES

We evaluated three variables that are known to influence tundra productivity: summer warmth index (SWI; the sum of all monthly mean temperatures >0°C, expressed as degree-months) (Walker et al. 2003; Raynolds et al. 2008; Berner et al. 2020), growing season precipitation (May–September) (Raynolds and Walker 2016; Kemppinen et al. 2019), spring sea ice concentration (Bhatt et al. 2010; Dutrieux et al. 2012; Macias-Fauria et al. 2017), and summer open water frequency. Data sources included satellite observations, station data, and gridded reanalysis datasets (Table 2). For spring sea ice concentration and summer open water frequency, we considered conditions in the east Bering Sea south of 63.5°N and within 100 km of the YKD coast. Across the full study area and for each physiographic unit, we calculated Pearson's correlation coefficients between variables for the period 2000–19 using linearly detrended time series, and assessed statistical significance using a two-tailed t test with reduced effective degrees of freedom from lag one autocorrelation (Santer et al. 2000).

TABLE 2. Summary of climate and cryospheric variables analyzed with respect to tundra vegetation productivity on the YKD.

Variable	Data source	Reference
Summer warmth index	AVHRR 8-day land surface temperature composites	Comiso (2003)
	Bethel Airport station data	Menne et al. (2012)
Precipitation	ERA5 reanalysis product	Hersbach et al. (2020)
	Bethel Airport station data	Menne et al. (2012)
Spring sea ice concentration	SSM/I	Comiso and Nishio (2008)
Summer open water	SSM/I	Comiso and Nishio (2008)

2) FIELD MEASUREMENTS OF VEGETATION

We referred to a network of field plots that provide context for interpreting NDVI trends on the YKD. Field data in the coastal and coastal plain units came from 55 long-term monitoring (LTM) plots that were established during 1995–98 (Jorgenson 2000) and resampled during 2007–10 and 2015–16. LTM plots were established in homogeneous vegetation patches and were 40–50 m^2 in size. During each sampling event, vegetation cover was sampled systematically using a vegetation point-intercept (VPI) method at 50 or 100 sample points (Karl et al. 2017). All vegetation and nonlive surfaces (e.g., bare soil and water) "hit" by a vertically mounted laser pointer were recorded at each point, providing quantitative vegetation metrics that are well correlated to NDVI and biomass (Jonasson 1988). From the VPI data, we calculated the mean live cover for three plant functional types (PFTs): shrub, herbaceous, and nonvascular (lichens and mosses) for field plots in coastal (n = 46 plots) and coastal plain (n = 9) physiography. We calculated live cover as the total number of hits for a PFT divided by the number of sample points, and thus can exceed 100% in multilayered canopies. We also referred to field verification plots that were sampled once using similar methods during 2017–18 in upland physiography on the central YKD (37 plots), and in deltaic physiography on the modern Yukon River Delta (53 plots).

3) DISTURBANCE HISTORY AND LOCAL OBSERVATIONS

YKD ecosystems experience a variety of ecological disturbances, many of which induce predictable responses in NDVI. We examined all MaxNDVI time series within the footprints of two common disturbances on the YKD: coastal flooding and tundra fire. Coastal flood extent mapping for three large storm-surge events (2005, 2006, and 2011) came from Terenzi et al. (2014), and tundra fire perimeters (1940–2018) came from the Alaska Interagency Coordination Center (AICC 2020). Finally, we considered expert knowledge shared by YKD elders concerning patterns of stability and change in the vicinity of three villages: Chevak in coastal and coastal plain physiography and Emmonak and Alakanuk in deltaic physiography (Fienup-Riordan et al. 2021). Local expert knowledge provides a source of site-specific observations of disturbances and vegetation change that predates the satellite record (Kokelj et al. 2012; Bronen et al. 2019).

4. Results

a. *NDVI seasonality analysis*

NDVI climatologies from MODIS indicate that regional differences in the timing of MaxNDVI exceed 1 month in tundra ecoregions of southwestern Alaska (Fig. 2). The timing of peak aboveground biomass varied along maritime-continental gradients; NDVI approaches peak (i.e., 95% of MaxNDVI) in late June in inland ecoregions (e.g., Nulato Hills) but not until late July in strongly maritime ecoregions (e.g., Bering Sea Islands). A similar pattern was evident within the YKD; physiographic units prevalent in inland areas (e.g., upland) greened up 1–2 weeks earlier than coastal units. Autumn senescence tends to begin first in continental ecoregions, but regional differences in autumn phenology are not as great as in spring and are not strongly reflected within physiographic units on the YKD. Overall, NDVI climatologies supported the use of observations during 1 July–31 August for calculating MaxNDVI and MedianNDVI on the YKD, a period that has been frequently used for NDVI studies elsewhere in the Arctic.

b. *NDVI trend analysis*

1) SPATIAL INTERCOMPARISON

All three records indicated net increases in MaxNDVI since 2000 on the YKD (Fig. 3). MODIS and Landsat recorded very similar patterns of trend; in both records, greening was prevalent in all physiographic units, and was most widespread in upland (59.8% and 60% of area, respectively) (Table 3). The MODIS and Landsat records also shared many trend "hot spots" in common throughout all physiographic units. The GIMMS record, however, indicated rather different hot spots of trend, primarily in coastal, coastal plain, and deltaic physiographic units. Browning was very limited in MODIS and Landsat time series (≤5% for most physiographic units) but was more extensive in the GIMMS record (>5% for all units), particularly in upland and riverine. All three records shared some trend hot spots that corresponded to disturbances related to tundra fire and coastal erosion. Although the MODIS and Landsat MaxNDVI records are similar, Landsat data gaps affected ≥50% of the total area of most physiographic units in 2010 and 2011 and introduce uncertainty relative to sensors with daily temporal resolution.

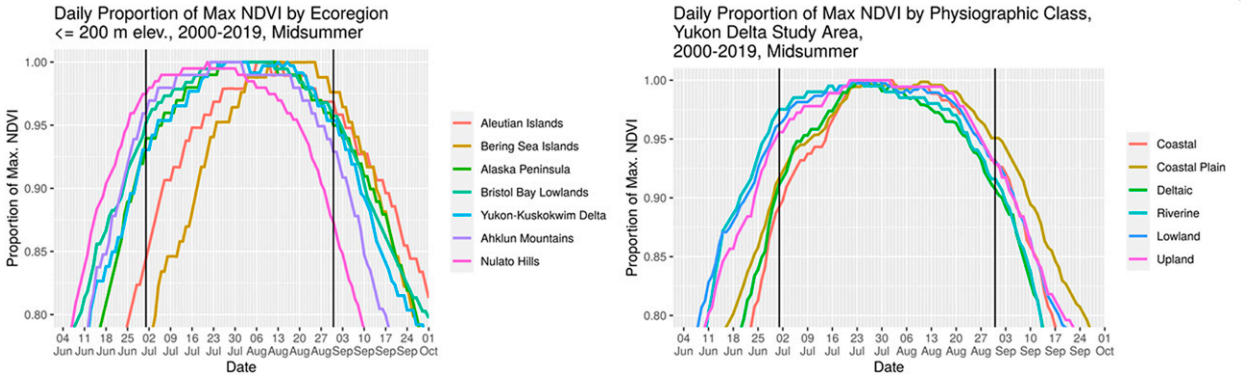

FIG. 2. NDVI climatologies derived from MODIS MCD43A4 adjusted reflectance for (left) southwestern Alaska ecoregions and (right) physiographic units on the YKD expressed as a proportion of MaxNDVI (2000–19). Ecoregions follow Nowacki et al. (2003) and are plotted from least to most continental. Vertical bars indicate 1 Jul–31 Aug.

Spatial patterns of MedianNDVI trend in the MODIS and Landsat records were very similar to those of MaxNDVI, although the extent of significant trends was somewhat lower. For GIMMS, MedianNDVI trends were more limited in extent than for MaxNDVI and were predominantly negative.

The TI-NDVI records from GIMMS and MODIS were dramatically different. MODIS indicated that TI-NDVI increase was nearly ubiquitous across the YKD during 2000–19 and was observed across >90% of deltaic and upland physiographic units (Table 4). In contrast, GIMMS indicated no trend in TI-NDVI over most of the region, with net declines evident in coastal, coastal plain, deltaic, and upland physiography.

2) TEMPORAL INTERCOMPARISON

GIMMS and MODIS time series of the regional average MaxNDVI displayed similar positive trends, but the GIMMS record was more variable and there were some striking disparities in some years (Fig. 4). In the MODIS record, MaxNDVI generally increased during 2000–07, decreased during 2008–11, and increased again in the last part of the record. GIMMS displayed similar patterns of interannual variability, except that no clear trend was evident in the first part of the record. The highest MaxNDVI values in the study period were all recorded in the last part of the record for both MODIS (2018–19) and GIMMS (2016–19). However, MaxNDVI values were strikingly different in 2000, the first year of the record.

For MedianNDVI, GIMMS and MODIS displayed weak negative and positive trends, respectively, and interannual variability was generally lower for both records than it was for MaxNDVI. Both MedianNDVI time series share similar patterns of variability, except that GIMMS recorded two strikingly low values in the middle part of the record (2010 and 2012).

TI-NDVI time series indicated a strong positive trend in the MODIS record but a weak negative trend in GIMMS. In the MODIS record, TI-NDVI increased markedly during 2000–04, generally decreased in 2005–13, and increased sharply during the last part of the record. In GIMMS, TI-NDVI generally declined during 2000–12 and was highly variable in the latter part of the record. Notably, the lowest and highest TI-NDVI values in the MODIS record were observed at the beginning (2000–01) and end (2016–19) of the record, respectively.

The GIMMS and MODIS records indicated predominantly positive trends in MaxNDVI across all physiographic units (Fig. 5), and patterns of interannual variability resembled those for the regional average MaxNDVI. The MODIS record for MedianNDVI was similar, although interannual variability and overall trends were weaker. GIMMS, however, indicated declining MedianNDVI for most physiographic units. MODIS observed strong positive trends in TI-NDVI across all physiographic units, but GIMMS recorded declining TI-NDVI across the three units associated with coastal areas; trends in the remaining, predominantly inland units were flat or slightly positive.

In both records, the mean values of MaxNDVI and MedianNDVI indicated that midsummer productivity was highest by far in the riverine and deltaic units, and the remaining four units were similar to one another. Patterns of variation were very different for TI-NDVI; full summer productivity was highest in riverine; intermediate for deltaic, lowland, and upland; and lowest in coastal and coastal plain.

3) SEASONALITY INTERCOMPARISON

GIMMS and MODIS indicated broadly similar NDVI seasonality over the YKD, with peak values occurring in July and August (Fig. 6). However, MODIS recorded positive trends in all seasonal periods, whereas GIMMS did not. While both records displayed increasing NDVI in June and early July, the records disagreed during shoulder seasons early and late in the growing season. Some of the sharpest increases in the MODIS record were evident during the spring greenup period in May, but GIMMS displayed virtually no trend. The records also differed later in the summer; GIMMS indicated weak declines in midsummer NDVI (i.e., late July and early August), whereas MODIS indicated weak increasing trends. By far the strongest disagreement is evident from October onward, although vegetation is dormant by this time of year and trends are presumably generated by variability in seasonal snow cover.

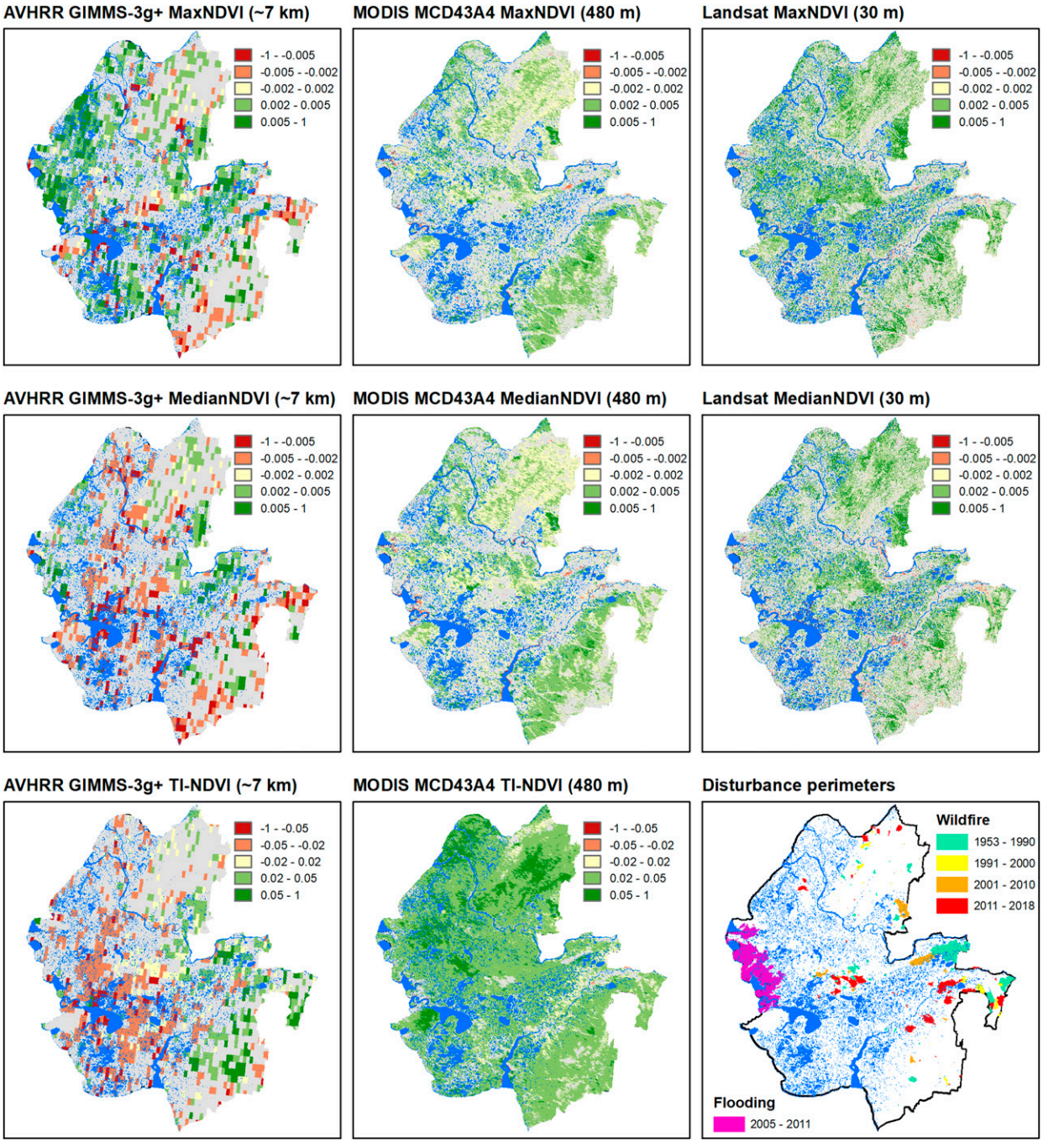

FIG. 3. Spatial intercomparison of trends for (top) MaxNDVI, (middle) MedianNDVI, and (bottom) TI-NDVI for (left) AVHRR GIMMS, (center) MODIS MCD43A4, and (right) Landsat TM/ETM+/OLI (MaxNDVI and MedianNDVI only) for 2000–19. Trends were calculated using robust regression; only trends with $p < 0.1$ are shown. The lower-right panel shows known tundra fire perimeters (AICC 2020), along with coastal lands inundated at least once during flood events of 2005, 2006, and 2011 for a portion of the central coast (Terenzi et al. 2014).

c. *Trend drivers*

1) CLIMATIC VARIABLES

The spaceborne and instrumental records for summer warmth displayed similar interannual variability, with low and record high SWI at the beginning and end of the study period, respectively (Fig. 7). However, SWI did not increase consistently during the intercomparison period; SWI exceeded 40°C months during 2002–07, declined below 40°C months during 2008–13, and then increased strongly at the

TABLE 3. Percentage of area greening, browning, or lacking trend for MaxNDVI in the GIMMS, MODIS, and Landsat records, by physiographic unit. Greening and browning trends are considered to be significant at $p < 0.1$.

	GIMMS			MODIS			Landsat		
Physiography	% green	% brown	% stable	% green	% brown	% stable	% green	% brown	% stable
Coastal	40.7	6.6	52.7	24.7	5.0	70.3	37.2	4.8	58.0
Coastal plain	43.9	9.4	46.7	39.3	1.4	59.3	49.3	2.7	47.9
Deltaic	31.5	7.2	61.3	57.5	1.0	41.5	38.1	4.0	57.9
Lowland	39.1	9.8	51.1	34.8	2.1	63.1	47.8	3.1	49.1
Riverine	33.0	12.7	54.4	25.8	2.3	71.9	24.0	9.4	66.6
Upland	25.4	14.4	60.2	59.8	0.5	39.7	60.0	1.5	38.5

end of the record, which included the two warmest summers in the spaceborne (since 1982) and instrumental records (Bethel Airport, since 1924). The regional average TI-NDVI for both GIMMS and MODIS had strong, positive correlations with AVHRR-observed SWI (Table 5); correlations were strongest for coastal, coastal plain, and deltaic physiographic units and diminished somewhat in the inland units (Tables S1–S6 in the online supplemental material). The regional average GIMMS MaxNDVI had a weaker, positive correlation with AVHRR SWI, but there was no correlation for MODIS MaxNDVI.

ERA5 indicated high interannual variability and no trend in growing season precipitation over the study period. Correlation analysis suggested negative correlations between growing season precipitation and both GIMMS and MODIS records for MaxNDVI and TI-NDVI, but none were significant. MODIS TI-NDVI was negatively correlated with precipitation in the coastal, coastal plain, and deltaic physiographic units (Tables S1–S3 in the online supplemental material), but no significant productivity correlations existed with precipitation over the full study area. Although agreement between ERA5 and the available instrumental record was poor during the NDVI intercomparison period, the two datasets were very similar during 1982–98; this shift was concurrent with automation of data collection at Bethel Airport. ERA5's correspondence with manned station observations provides confidence in this reanalysis dataset, which improves upon previous products for the Arctic and is less prone to discontinuities than are station observations in Alaska (White et al. in 2021).

The SSM/I sea ice record showed very high interannual variability in spring sea ice concentration off the YKD coast. Spring sea ice concentration generally increased during the first part of the study period but declined sharply after 2013, and the two lowest values were recorded at the end of the study period. Sea ice concentrations were comparatively high for six consecutive years in the middle of the study period (2008–13). GIMMS and especially MODIS TI-NDVI displayed strong negative correlations with spring sea ice concentration for the full study area; as for SWI, these correlations tended to be strongest for the coastal, coastal plain, and deltaic physiographic units.

2) FIELD MEASUREMENTS OF VEGETATION

Long-term vegetation measurements indicated contrasting changes in live vegetation cover since the mid-1990s in coastal and coastal plain physiography. At coastal plots ($n = 46$), total cover was highest in the late (2015–16) sampling period (Fig. 8). Herbaceous vegetation (primarily sedges) formed most of the live cover in all periods; increases in herb abundance after the middle (2007–10) sampling period accounted for most of the change in live cover over time. Shrub cover was also highest in the most recent sampling period, but shrubs were not abundant and were absent from about half of coastal plots.

In coastal plain physiography, total live cover at plots ($n = 9$) was highest in the middle and late sampling periods. In all sampling periods, nonvascular plants formed the majority of the live cover. Cover of live shrubs and nonvascular plants declined in the late sampling period, but herbaceous cover was similar throughout the study period.

3) DISTURBANCE HISTORY

The coastal flood extent mapping of Terenzi et al. (2014) delineated peak saltwater inundation during fall storms in

TABLE 4. As in Table 3, but for TI-NDVI in the GIMMS and MODIS records, by physiographic unit. Greening and browning trends are considered to be significant at $p < 0.1$.

	GIMMS			MODIS		
Physiography	% green	% brown	% stable	% green	% brown	% stable
Coastal	5.9	24.9	69.2	74.0	0.3	25.7
Coastal plain	1.9	33.0	65.1	81.1	0.1	18.8
Deltaic	0.3	24.4	75.3	94.4	0.5	5.0
Lowland	26.9	20.7	52.4	87.6	0.2	12.2
Riverine	24.9	20.6	54.5	82.5	0.4	17.1
Upland	17.6	20.8	61.6	92.2	0.1	7.7

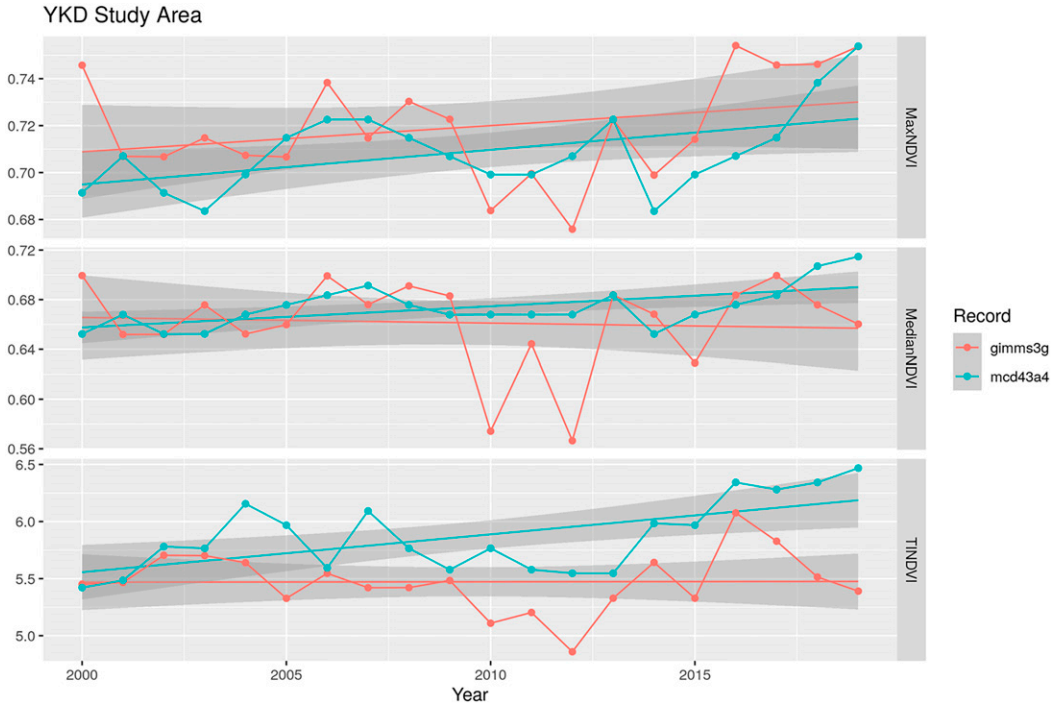

FIG. 4. Time series intercomparison of the regional average (top) MaxNDVI, (middle) MedianNDVI, and (bottom) TI-NDVI for GIMMS and MODIS. Time series are not shown for Landsat sensors because of excessive data gaps.

2005, 2006, and 2011 in a 6700-km^2 portion of the central YKD coast. Flooding primarily affected coastal physiography; nonflooded areas primarily corresponded to coastal plain and upland. MaxNDVI displayed no trend in flood-affected areas for all three sensors, and there were no obvious changes in MaxNDVI in the summers after the three flood events. However, MODIS and Landsat did record increasing MaxNDVI in adjacent nonflooded areas. The Landsat record displayed much higher interannual variability, but years with abrupt changes in MaxNDVI were evident in both flooded and nonflooded areas, and this variability was not clearly associated with flood disturbance.

The fire perimeter database (AICC 2020) indicated that at least 4615 km^2 (4.7%) of the YKD has experienced tundra fire since 1940. Over half of this fire activity occurred during the 2000–19 study period, primarily in upland physiography. Wildfire disturbance and postfire successional processes were generally obvious in the Landsat MaxNDVI record, although this record also has high interannual variability that is likely attributable to data gaps (Fig. 9). Tundra that burned circa 2005—near the beginning of the study period—displayed the strongest greening in the Landsat record, although greening was also evident in unburned areas. MaxNDVI dropped after 2015 burns in all records, with the magnitude of decline proportional to the spatial resolution of each sensor. There were also sharp increases in MODIS and Landsat MaxNDVI after 2015 fire, but this was not evident in GIMMS. Across all analyzed areas, MODIS and Landsat displayed MaxNDVI trends of the same sign and similar magnitude, whereas GIMMS trends were often different.

5. Discussion

a. *Intercomparison of time series*

Do the three satellite records agree on NDVI trends in terms of sign, magnitude, and spatiotemporal pattern during 2000–19? Our intercomparison revealed mixed patterns of agreement among the GIMMS, MODIS, and Landsat records, similar to earlier continental-scale studies (e.g., Guay et al. 2014; Ju and Masek 2016). All records showed increasing trends in MaxNDVI on the YKD, but greening was far more extensive in the MODIS and Landsat records than in GIMMS. MODIS and Landsat also shared very similar spatial patterns of MaxNDVI trend, whereas "hot spots" of trend in GIMMS generally did not overlap those of the other records. Widespread MaxNDVI increases observed by MODIS and Landsat in uplands—the most extensive physiographic unit—are particularly notable because these areas are unlikely to be affected by surface water variability, which reduces the signal to noise ratio in NDVI time series and can confound trend attribution in wetland areas (Raynolds and Walker 2016). The MODIS and Landsat records were also very similar in other physiographic units. Although the low temporal resolution of Landsat limits its comparability with GIMMS and MODIS on annual time scales, the spatial similarity of Landsat and MODIS-observed trends over the full study period is striking. These independent datasets corroborate one another and indicate that recent MaxNDVI increases on the YKD have been more extensive than the GIMMS record would suggest; Landsat has also indicated more widespread greening than GIMMS at circumpolar scales through 2016 (Berner et al. 2020).

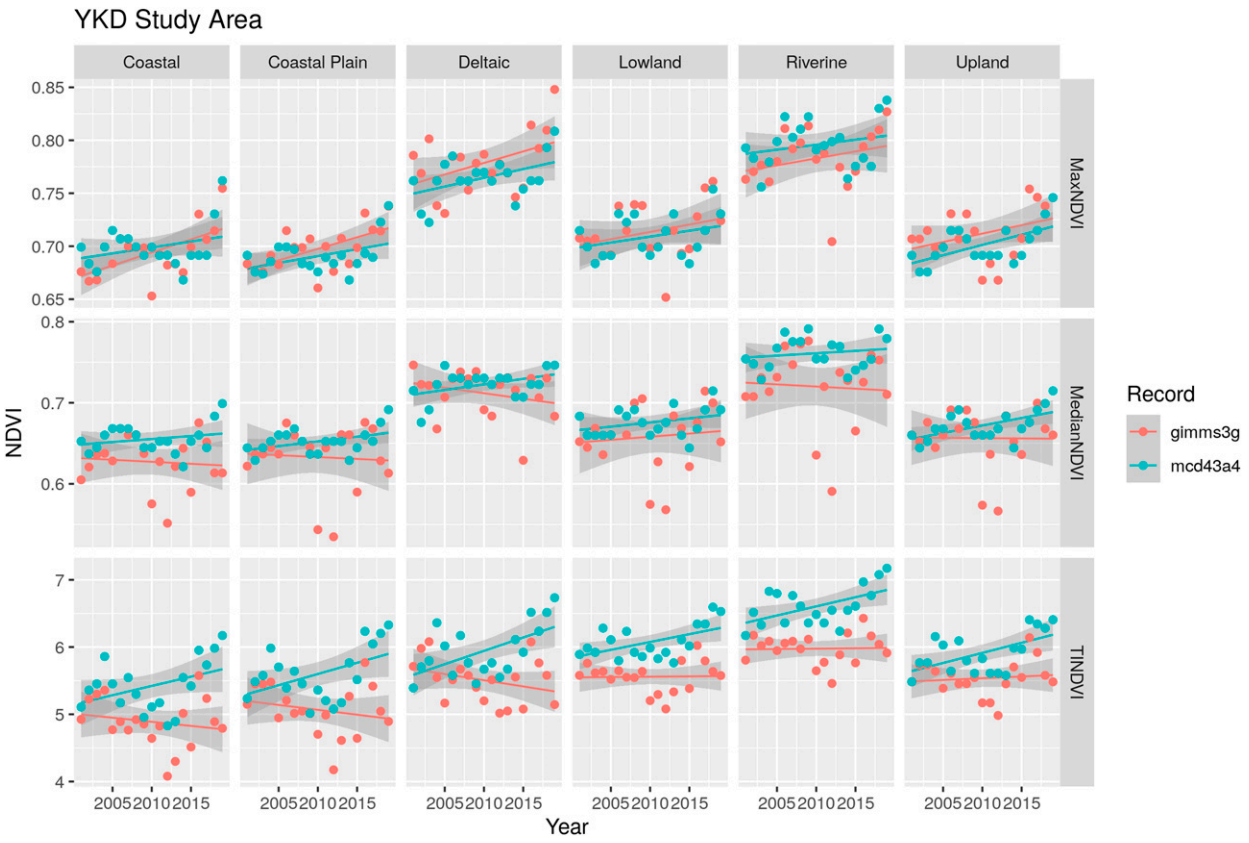

FIG. 5. As in Fig. 4, but stratified by physiographic unit.

MedianNDVI is generally the most appropriate greenness metric for analysis of the Landsat record, given Landsat's low temporal resolution, data gaps, and the resulting tendency for MaxNDVI to be biased high in years with more clear-sky observations. Nonetheless, the MODIS and Landsat records for MedianNDVI were very similar to one another, and to MaxNDVI trends for these sensors. This provides additional corroborating evidence of increasing midsummer greenness on the YKD. The GIMMS record for MedianNDVI instead showed a weak decline in MedianNDVI; however, MedianNDVI is of questionable validity for GIMMS, because this metric is simply the median of four maximal values observed during bimonthly periods of July and August.

The GIMMS and MODIS records for TI-NDVI displayed the most striking differences by far in both magnitude and sign, particularly at the end of the intercomparison period. The MODIS record showed increasing TI-NDVI across >88% of the YKD, and positive trends prevailed across all physiographic units. Decreasing trends were of very limited extent in the MODIS record and were clearly linked to contiguous areas affected by disturbances such as tundra fire and coastal erosion. Significant TI-NDVI trends were far less extensive in the GIMMS record, and the trends that were evident were predominantly negative. Our intercomparison thus calls into question the validity of the regional decline in TI-NDVI observed by GIMMS over the YKD.

The seasonal and interannual variability of tundra greenness provides context concerning possible sources of disagreement in the TI-NDVI records. Patterns of interannual variation in MaxNDVI were broadly similar between the records, with the highest values clustered at the end of both records, and with similar sequences of low and high values alternating at periods of about five years. However, the GIMMS record displayed much higher interannual variability, and GIMMS MaxNDVI was strikingly different in a few years—especially in 2000, the beginning of the intercomparison period. This highlights the difficulty of assessing the ecological significance of trends in noisy time series that are subject to high interannual variability. Nonetheless, the area-averaged MaxNDVI trends observed by GIMMS and MODIS agree in sign and are similar in magnitude. This provides confidence that peak productivity has in fact increased over the 20 year study period and suggests that disagreement between the GIMMS and MODIS records for TI-NDVI is generally not attributable to observations made in midsummer.

Why, then, might the TI-NDVI records be so different? Short snow-free seasons and high cloud frequency make the analysis and interpretation of Arctic NDVI time series challenging in general. However, the YKD is one of the circumpolar region's most maritime areas, with a prolonged snow-free season, variable winter sea ice and snow cover, and very high cloud frequency. Although both MODIS and

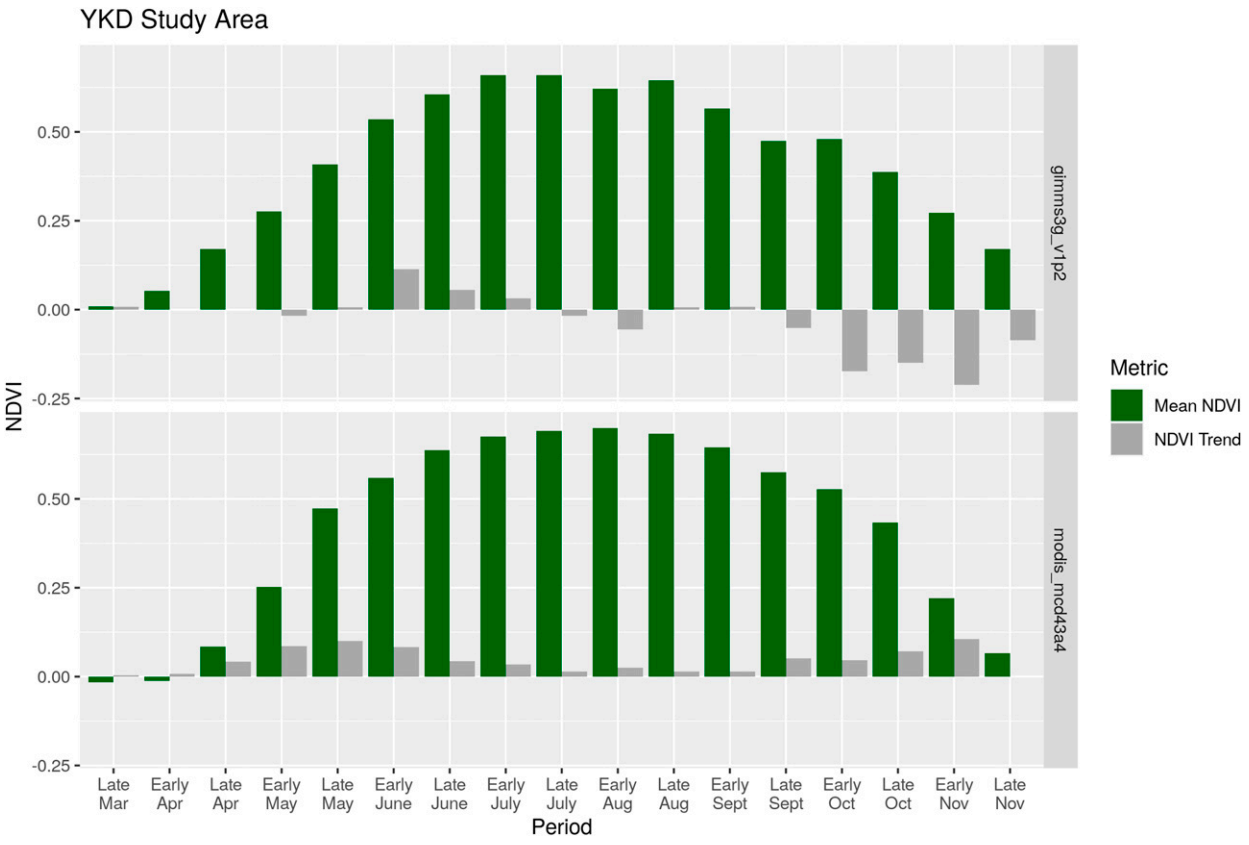

FIG. 6. Climatology and trends of bimonthly NDVI evident in (top) AVHRR GIMMS and (bottom) MODIS MCD43A4 for 2000–19. Trends are calculated using linear regression.

GIMMS observed similar, positive greenness trends in early summer (1 June–15 July), agreement was poor in other periods, especially in spring (1–31 May), a pattern that has also been identified in global intercomparisons of NDVI seasonality (Ye et al. 2021). GIMMS-observed declines in spring NDVI on the YKD are puzzling, given the dramatic decline in spring sea ice and increases in land surface temperatures at the end of the record. In addition, the seasonal climatology of GIMMS displays fluctuating NDVI in late summer and fall compositing periods, when we would expect NDVI to decline monotonically. Although the YKD experiences high cloud frequency throughout the growing season, cloud frequency is highest in late summer and fall as in many other Arctic regions (Taylor et al. 2019), and continued decline in spring sea ice may be accompanied by increased cloudiness at that season also (Palm et al. 2010). Given that TI-NDVI incorporates observations from shoulder seasons when NDVI is well below peak, and there is partial snow cover (spring) and very high cloud frequency (late summer–fall) at these times of year, a simple explanation is that GIMMS is more vulnerable to subpixel effects, particularly given its coarse spatial resolution. This limitation is likely to be most pronounced in regions with long snow-free seasons and high cloud frequency, such as in maritime Arctic regions like the YKD, potentially compounding noise arising from AVHRR's lack of onboard calibration and inconsistencies among the many instruments that have contributed to the record.

b. *Assessment of climate drivers*

What is the relative importance of summer temperature, precipitation, and spring sea ice extent in controlling tundra vegetation productivity on the YKD, and do these relationships clarify which record(s) are most reliable? Given that GIMMS and MODIS TI-NDVI trends were dramatically different, it is noteworthy that the detrended records shared similar, strong correlations with spring sea ice concentration and summer warmth. For example, three of the coldest summers during the study period (2010–12) coincided with the lowest TI-NDVI values in the GIMMS record. However, the correspondence between GIMMS TI-NDVI and SWI appeared to break down late in the record when a sequence of very warm summers was accompanied by decreasing TI-NDVI. Although early snowmelt and summer drying have been linked to browning in parts of the Arctic (e.g., Gamon et al. 2013; Verdonen et al. 2020), the very strong positive trends in the MODIS TI-NDVI record—including the record warm summers of 2016 and 2019—suggest a straightforward relationship between summer warmth and vegetation productivity on the YKD. Positive correlations between MODIS

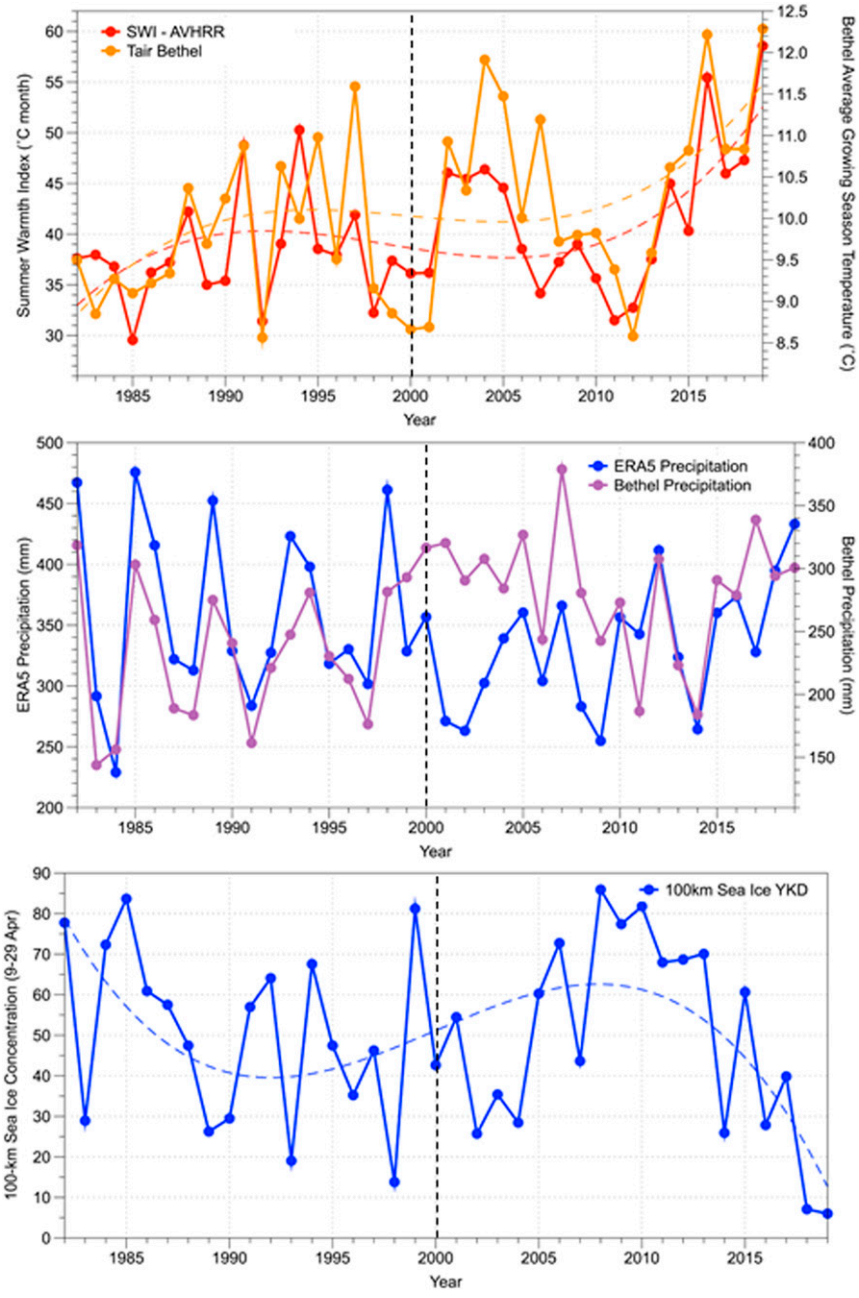

FIG. 7. Regionally averaged (top) SWI, (middle) summer precipitation, and (bottom) spring sea ice concentration for 1982–2019. The instrumental record at Bethel Airport is plotted with the spaceborne SWI and ERA5 precipitation reanalysis records. Sea ice concentration is summarized for 9–29 Apr, which is centered on the typical week that sea ice concentration falls below 50% in the eastern Bering Sea. Linear, quadratic, and cubic fits were compared, and cubic was chosen (dashed lines) to maximize R^2 and minimize root-mean-square error. The dashed vertical line marks the beginning of the NDVI intercomparison period (2000).

TI-NDVI and summer warmth were strongest in coastal, coastal plain, and deltaic physiography, but these units include extensive waterbodies, raising the question of whether correlations in coastal areas were inflated due to masking of water. However, considering that water occurrence is similar in the inland lowland and riverine units, we argue that differences in the relationship between TI-NDVI and summer warmth along coast–inland gradients were not artifacts of water masking. Although NDVI metrics were not significantly correlated with summer precipitation over the full

TABLE 5. Correlations among the regional average NDVI metrics and SWI, summer precipitation, spring sea ice concentration, and summer open water for 2000–19. Significant correlations are indicated with boldface type ($p \leq 0.05$). SI = sea ice concentration, OW = summer open water, and TSP = total summer precipitation (June–August).

			SWI		MaxNDVI		TI-NDVI		
Variable	SI	OW	AVHRR	ERA5	GIMMS	MODIS	GIMMS	MODIS	TSP
SI	1	**−0.84**	**−0.74**	−0.3	−0.37	−0.07	**−0.55**	**−0.71**	0.15
OW		1	**0.74**	0.32	0.35	−0.15	**0.69**	**0.74**	−0.09
SWI AVHRR			1	0.21	**0.5**	0.12	**0.7**	**0.75**	−0.14
SWI ERA5				1	0.11	0.11	0.26	0.11	−0.35
MaxNDVI GIMMS					1	**0.44**	**0.62**	0.35	−0.23
MaxNDVI MODIS						1	−0.15	0.21	−0.33
TI-NDVI GIMMS							1	**0.57**	−0.40
TI-NDVI MODIS								1	−0.32
TSP									1

study area, MODIS TI-NDVI was negatively correlated with precipitation in coastal, coastal plain, and deltaic physiographic units. Collectively, these results indicate that YKD tundra productivity is generally not limited by moisture.

Although the YKD experiences a mild climate and long open-water season as compared with most other circumpolar regions, the climatic drivers of TI-NDVI on the YKD appear to be similar to colder parts of the Arctic, such as northwestern Siberia and Alaska's North Slope (Macias-Fauria et al. 2012; Dutrieux et al. 2012; Miles and Esau 2016; Reichle et al. 2018). Increasing tundra productivity has also been linked to increasing growing season length in many Arctic regions (Xu et al. 2013; Park et al. 2016; Arndt et al. 2019). However, browning has been observed over many tundra regions in recent years, and this has contributed to a more complex picture of Arctic greening (Park et al. 2016; Myers-Smith et al. 2020). For example, although our intercomparison did not corroborate GIMMS-observed browning over the YKD, MODIS *does* corroborate browning in non-Arctic tundra elsewhere in southwestern Alaska (Potter and Alexander 2020). Extreme events during winter, such as rain-on-snow (ROS) and winter thaw events, are becoming more frequent (Graham et al. 2017) and have been linked to abrupt productivity declines in maritime tundra of the Barents Sea (Bokhorst et al. 2011; Bjerke et al. 2014). The YKD experiences frequent ROS (Bieniek et al. 2018) and such events have long been considered to be common by YKD elders. Although we did not include such drivers in our analysis, and accurate spaceborne measures of circumpolar snow cover remain elusive, the overwhelmingly positive trends in MODIS-observed NDVI for all bimonthly periods, coupled with strong positive correlations between TI-NDVI and summer warmth for both GIMMS and MODIS records, suggest that summer warmth has been a simple and consistent predictor of regional TI-NDVI trends on the YKD since 2000.

c. *Assessment of landscape-scale drivers*

Do observed plot-scale dynamics (~1994–2016), landscape-scale disturbance records, and testimonials from YKD elders corroborate the satellite record(s)? Upland landscapes of the YKD have experienced extensive wildfire in recent decades, and these burns permit a first-order assessment of whether satellite records conform to the expected response of NDVI to disturbance. The MODIS and Landsat records largely reflected the expected NDVI responses within the wildfire

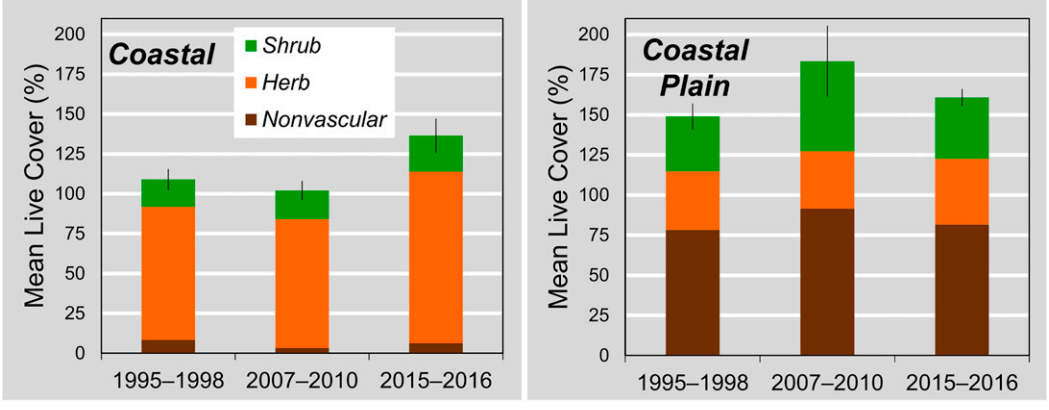

FIG. 8. Summaries of mean live cover of shrubs, herbs, and nonvascular plants at long-term monitoring plots in (left) coastal and (right) coastal plain physiography measured during three sampling periods for 1995–2016. Black lines indicate standard errors for mean total live cover.

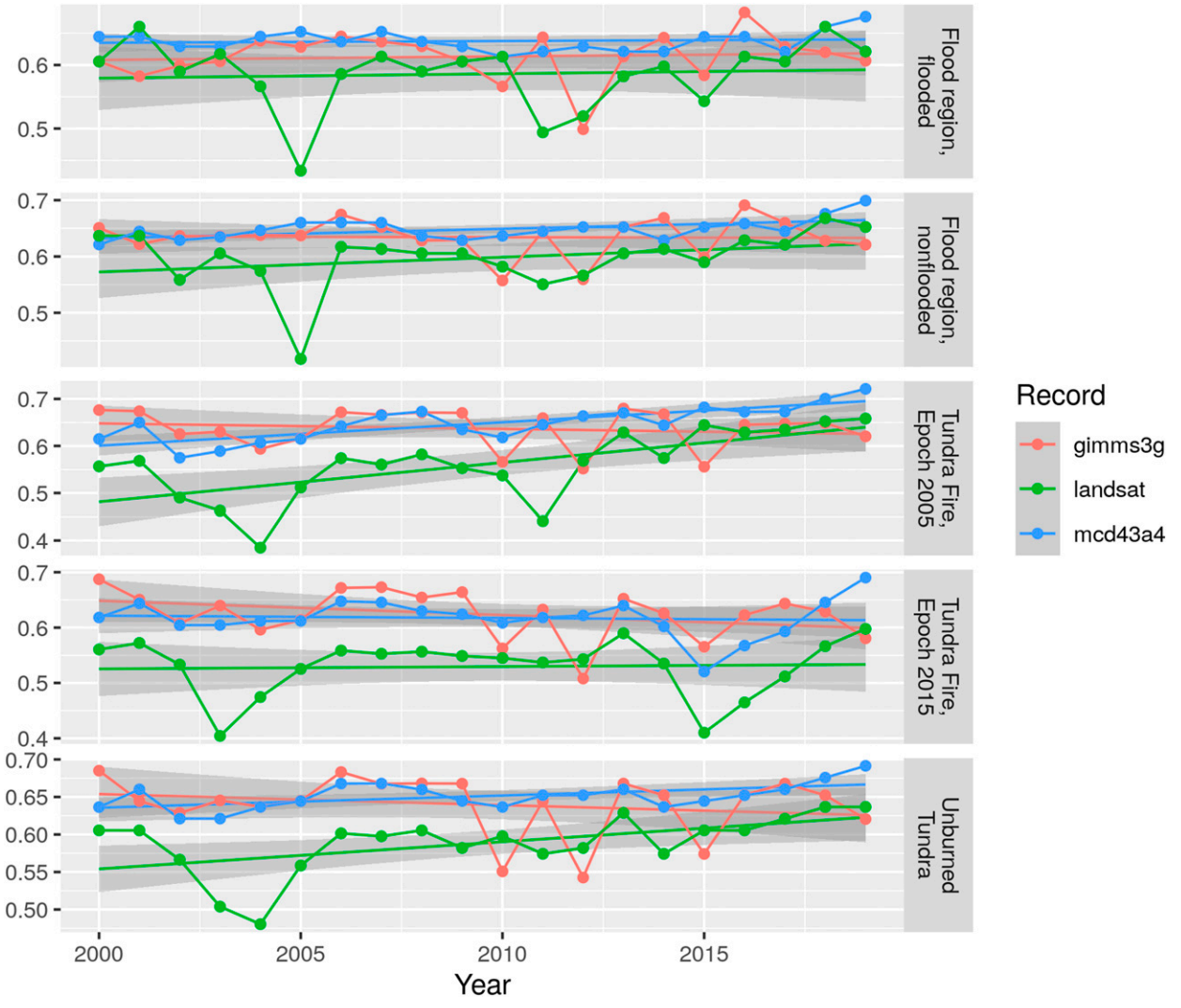

FIG. 9. Intercomparison of MaxNDVI time series for areas affected by coastal flooding and tundra fire and for adjacent undisturbed areas.

perimeters based on fire timing, and this lends confidence to the overall NDVI trends evident in these two datasets. The GIMMS record did not clearly reflect expected greenness responses to fire, although its low spatial resolution complicates attempts to validate it within the relatively small footprints of burns on the YKD.

We also referred to field-based LTM data and knowledge exchange with YKD elders to evaluate changes in land surface conditions that could account for comparatively subtle greenness trends in undisturbed landscapes of the YKD. Although the LTM data came from a relatively small area, and individual field plots were far smaller than the footprint of a single MODIS or GIMMS pixel, few comparable datasets exist by which to relate in situ measurements of vegetation cover to multidecadal satellite data. The YKD's coastal ecosystems are disproportionately influenced by fall storms and extreme weather, but none of the satellite records displayed abrupt changes in NDVI associated with 3 coastal flood events that occurred during the study period. In fact, the LTM dataset suggested that live cover tended to increase after these events in coastal physiography, possibly because the sedge-dominated vegetation is adapted to saline conditions and sedimentation provides a source of soil nutrients. We found no clear trend in vegetation cover in coastal plain, although we did observe local mortality of shrubs due to saltkill, as well as ground subsidence caused by permafrost thaw (Whitley et al. 2018).

Reports from YKD elders provide intriguing evidence of vegetation changes both during the intercomparison period, and entirely preceding the satellite record. These reports provide evidence of stress or dieback of herbaceous and shrub species sought for berry harvest in several physiographic settings (Herman-Mercer et al. 2020). However, the overwhelming consensus among residents of the central coast region and the Yukon River Delta is that there has been a long-term increase in the density and stature of vegetation. This has been particularly obvious on the modern Yukon River Delta, where

residents have reported widespread increase in tall alder (*Alnus*) and willow (*Salix*) in recent decades (Rearden and Fienup-Riordan 2014). This shrub expansion has been accompanied by the recent immigration of moose, which were not known to inhabit the region before 1940 but have since become an important subsistence resource (Perry 2010). Spatial patterns of MODIS and Landsat-observed MaxNDVI indicate the most widespread greening in upland and deltaic environments; this pattern is consistent with shrubification because shrubs are common and usually form the top of the canopy in these physiographic classes.

d. Synthesis

Spaceborne NDVI datasets are indispensable for circumpolar monitoring of vegetation in a warming Arctic, but NDVI signals are also influenced by other surface and atmospheric properties. Consequently, identifying the salient processes that underlie complex spatiotemporal trends requires the integration of a broad base of information. On the YKD, we considered disparate remote sensing, reanalysis, field datasets, and local expert knowledge to interpret 20 years of concurrent spaceborne observations from different sensors. What do our findings mean in a circumpolar context, and what might we do differently in the future? The GIMMS record is exceptional for its longevity and global coverage but is prone to several sources of noise that can produce idiosyncratic spatiotemporal trends. Our intercomparison indicated that GIMMS is especially prone to noise during shoulder seasons, when tundra landscapes hold patchy seasonal snow and are usually obscured by clouds. Nonetheless, the GIMMS TI-NDVI record was well correlated with summer warmth, which indicates it remains a valuable dataset particularly when the full record (now 39 years) is considered. Our intercomparison only examined the latter half of the record, and although MODIS and Landsat did not corroborate GIMMS over this time period, the strong increases in NDVI observed by modern sensors suggests that tundra ecosystems of the YKD are responding positively to warming, and long-term Arctic greening trends evident in the full GIMMS record remain valid. Going forward, MODIS has obvious advantages for trend analysis across multiple spatial scales. The MODIS period-of-record now exceeds 20 years, which is comparable to that of the GIMMS record when the first seminal reports of Arctic greening emerged (e.g., Myneni et al. 1997; Jia et al. 2003).

In a circumpolar context, the YKD is challenging for evaluating trends and their underlying drivers because it experiences exceptionally high variability in spring sea ice extent and temperature, as well as frequent storms, coastal flooding, and winter thaw events. On the other hand, the MODIS record indicates steady increases in TI-NDVI over the last 20 years, with a straightforward relationship with summer temperatures. MODIS and Landsat also share very similar positive trends in MaxNDVI, and although MaxNDVI was not well correlated with summer warmth on the YKD, the circumpolar Landsat record displays widespread positive correlations with summer warmth (Berner et al. 2020). Although differences in source datasets, study periods, and data processing methods make it difficult to directly compare NDVI trend analyses, the preponderance of greening in circumpolar MODIS and Landsat datasets suggests that the broadscale drivers of Arctic greening may be more straightforward than GIMMS-based assessments would indicate.

Arctic deltas have become a focal point of recent research (Lantz et al. 2015; Nitze and Grosse 2016; Lauzon et al. 2019), but the YKD is distinctive in that it has a much milder climate, permafrost is discontinuous, and the permafrost that is present is at high risk of thawing within the next several decades (Pastick et al. 2015; Jorgenson et al. 2018). Ongoing Arctic warming and diminishing sea ice suggest that the high climatic variability currently being observed on the YKD could become common in other parts of the Arctic in the future (Lawrence et al. 2008; Dobricic et al. 2020; Landrum and Holland 2020). The dramatic decline in spring sea ice offshore, and the discontinuous and declining extent of permafrost onshore make the YKD a ''black sheep'' in a circumpolar context, given the strong influence that the cryosphere has on regional- and landscape-scale NDVI dynamics elsewhere in the Arctic. This raises the questions of whether and for how long maritime areas of the circumpolar region such as the YKD will fit historical concepts of ''what is Arctic.''

Acknowledgments. This research was part of the National Aeronautics and Space Administration (NASA) Arctic Boreal Vulnerability Experiment (ABoVE), Contract NNH16CP09C. We thank YKD elders and other residents in the villages of Chevak, Emmonak, and Alakanuk for sharing their knowledge of environmental conditions and change, and we thank Ann Fienup-Riordan, Mark John, and Rebecca Nayamin-Kelly for their assistance in organizing discussions. We are also grateful to James Ayuluk and Jake Redfox for helping us safely access field sites. Spencer Rearden and Brian McCaffery at the Yukon Delta National Wildlife Refuge, Jeff Estensen and Mick Leach at the Alaska Department of Fish and Game, and Ryan Choi at Utah State University provided logistical support for field studies. We also thank Peter A. Bieniek for his helpful comments on the paper.

Data availability statement. The spaceborne and instrumental datasets that we analyzed are in the public domain and freely available from online data portals. Trend analyses and underlying spatial datasets will be available at the Oak Ridge Laboratory Distributed Active Archive Center (ORNL-DAAC) within 2 months of publication.

REFERENCES

AICC, 2020: Alaska wildland fire information map series: Fuels and fire history. https://fire.ak.blm.gov/.

Arndt, K. A., and Coauthors, 2019: Arctic greening associated with lengthening growing seasons in northern Alaska. *Environ. Res. Lett.*, **14**, 125018, https://doi.org/10.1088/1748-9326/ab5e26.

Atkinson, D. E., 2005: Observed storminess patterns and trends in the circum-Arctic coastal regime. *Geo-Mar. Lett.*, **25**, 98–109, https://doi.org/10.1007/s00367-004-0191-0.

Beck, H. E., T. R. McVicar, A. I. J. M. van Dijk, J. Schellekens, R. A. M. de Jeu, and L. A. Bruijnzeel, 2011: Global evaluation of four AVHRR–NDVI data sets: Intercomparison and

assessment against Landsat imagery. *Remote Sens. Environ.*, **115**, 2547–2563, https://doi.org/10.1016/j.rse.2011.05.012.

Berner, L. T., and Coauthors, 2020: Summer warming explains widespread but not uniform greening in the Arctic tundra biome. *Nat. Commun.*, **11**, 4621, https://doi.org/10.1038/s41467-020-18479-5.

Bhatt, U. S., and Coauthors, 2010: Circumpolar Arctic tundra vegetation change is linked to sea ice decline. *Earth Interact.*, **14**, https://doi.org/10.1175/2010EI315.1.

——, and Coauthors, 2013: Recent declines in warming and vegetation greening trends over Pan-Arctic tundra. *Remote Sens.*, **5**, 4229–4254, https://doi.org/10.3390/rs5094229.

——, and Coauthors, 2017: Changing seasonality of panarctic tundra vegetation in relationship to climatic variables. *Environ. Res. Lett.*, **12**, 055003, https://doi.org/10.1088/1748-9326/aa6b0b.

Bieniek, P. A., and Coauthors, 2015: Climate drivers linked to changing seasonality of Alaska coastal tundra vegetation productivity. *Earth Interact.*, **19**, https://doi.org/10.1175/EI-D-15-0013.1.

——, U. S. Bhatt, J. E. Walsh, R. Lader, B. Griffith, J. K. Roach, and R. L. Thoman, 2018: Assessment of Alaska rain-on-snow events using dynamical downscaling. *J. Appl. Meteor. Climatol.*, **57**, 1847–1863, https://doi.org/10.1175/JAMC-D-17-0276.1.

Bjerke, J. W., S. Rune Karlsen, K. Arild Høgda, E. Malnes, J. U. Jepsen, S. Lovibond, D. Vikhamar-Schuler, and H. Tømmervik, 2014: Record-low primary productivity and high plant damage in the Nordic Arctic region in 2012 caused by multiple weather events and pest outbreaks. *Environ. Res. Lett.*, **9**, 084006, https://doi.org/10.1088/1748-9326/9/8/084006.

Bokhorst, S. F., J. W. Bjerke, H. Tømmervik, T. V. Callaghan, and G. K. Phoenix, 2009: Winter warming events damage sub-Arctic vegetation: Consistent evidence from an experimental manipulation and a natural event. *J. Ecol.*, **97**, 1408–1415, https://doi.org/10.1111/j.1365-2745.2009.01554.x.

——, ——, L. E. Steet, T. V. Callaghan, and G. K. Phoenix, 2011: Impacts of multiple extreme winter warming events on sub-Arctic heathland: Phenology, reproduction, growth, and CO_2 flux responses. *Global Change Biol.*, **17**, 2817–2830, https://doi.org/10.1111/j.1365-2486.2011.02424.x.

Bronen, R., D. Pollock, J. Overbeck, D. Stevens, S. Natali, and C. Maio, 2019: Usteq: Integrating indigenous knowledge and social and physical sciences to coproduce knowledge and support community-based adaptation. *Polar Geogr.*, **43** (2–3), 1–18, https://doi.org/10.1080/1088937X.2019.1679271.

CAVM Team, 2003: Circumpolar Arctic vegetation map (1: 7,500,000 scale). Conservation of Arctic Flora and Fauna (CAFF) Map No. 1, U.S. Fish and Wildlife Service, https://www.geobotany.uaf.edu/cavm/.

Clinton, N., 2020: Non-parametric trend analysis. Google Earth Engine, accessed 22 April 2021, https://developers.google.com/earth-engine/tutorials/community/nonparametric-trends.

Comiso, J. C., 2003: Warming trends in the Arctic from clear sky satellite observations. *J. Climate*, **16**, 3498–3510, https://doi.org/10.1175/1520-0442(2003)016<3498:WTITAF>2.0.CO;2.

——, and F. Nishio, 2008: Trends in the sea ice cover using enhanced and compatible AMSR-E, SSM/I, and SMMR data. *J. Geophys. Res.*, **113**, C02S07, https://doi.org/10.1029/2007JC004257.

Dobricic, S., S. Russo, L. Pozzoli, J. Wilson, and E. Vignati, 2020: Increasing occurrence of heat waves in the terrestrial Arctic. *Environ. Res. Lett.*, **15**, 024022, https://doi.org/10.1088/1748-9326/ab6398.

Dutrieux, L. P., H. Bartholomeus, M. Herold, and J. Verbesselt, 2012: Relationships between declining summer sea ice, increasing temperatures and changing vegetation in the Siberian Arctic tundra from MODIS time series (2000–11). *Environ. Res. Lett.*, **7**, 044028, https://doi.org/10.1088/1748-9326/7/4/044028.

Fienup-Riordan, A., 1999: *Yaqulget qaillun pilartat* (what the birds do): Yup'ik Eskimo understanding of geese and those who study them. *Arctic*, **52** (1), 1–22, https://doi.org/10.14430/arctic905.

——, G. V. Frost, R. Nayamin-Kelly, U. S. Bhatt, A. S. Hendricks, M. John, and P. Odom, 2021: Yup'ik and Cup'ik observations of Alaska's changing Yukon-Kuskokwim Delta: Results of a knowledge exchange meeting with natural scientists. ABR, Inc.—Environmental Research & Services Rep., 40 pp., https://doi.org/10.3334/ORNLDAAC/1894.

Gamon, J. A., K. F. Huemmrich, R. S. Stone, and C. E. Tweedie, 2013: Spatial and temporal variation in primary productivity (NDVI) of coastal Alaskan tundra: Decreased vegetation growth following earlier snowmelt. *Remote Sens. Environ.*, **129**, 144–153, https://doi.org/10.1016/j.rse.2012.10.030.

Gill, R. E., Jr., and C. M. Handel, 1990: The importance of subarctic intertidal habitats to shorebirds: A study of the central Yukon-Kuskokwim Delta, Alaska. *Condor*, **92**, 709–725, https://doi.org/10.2307/1368690.

Gorelick, N., M. Hancher, M. Dixon, S. Ilyushchenko, D. Thau, and R. Moore, 2017: Google Earth Engine: Planetary-scale geospatial analysis for everyone. *Remote Sens. Environ.*, **202**, 18–27, https://doi.org/10.1016/j.rse.2017.06.031.

Graham, R. M., L. Cohen, A. A. Petty, L. N. Boisvert, A. Rinke, S. R. Hudson, M. Nicolaus, and M. A. Granskog, 2017: Increasing frequency and duration of Arctic winter warming events. *Geophys. Res. Lett.*, **44**, 6974–6983, https://doi.org/10.1002/2017GL073395.

Grebmeier, J. M., and Coauthors, 2006: A major ecosystem shift in the northern Bering Sea. *Science*, **311**, 1461–1464, https://doi.org/10.1126/science.1121365.

Guay, K. C., P. S. A. Beck, L. T. Berner, S. J. Goetz, A. Baccini, and W. Buermann, 2014: Vegetation productivity patterns at high northern latitudes: A multi-sensor satellite data assessment. *Global Change Biol.*, **20**, 3147–3158, https://doi.org/10.1111/gcb.12647.

Herman-Mercer, N. M., M. Laituri, M. Massey, E. Matkin, R. Toohey, K. Elder, P. F. Schuster, and E. Mutter, 2019: Vulnerability of subsistence systems due to social and environmental change: A case study in the Yukon-Kuskokwim Delta, Alaska. *Arctic*, **72**, 258–272, https://doi.org/10.14430/arctic68867.

——, R. A. Loehman, R. C. Toohey, and C. Paniyak, 2020: Climate- and disturbance-driven changes in subsistence berries in coastal Alaska: Indigenous knowledge to inform ecological inference. *Hum. Ecol.*, **48**, 85–99, https://doi.org/10.1007/s10745-020-00138-4.

Hersbach, H., and Coauthors, 2020: The ERA5 global reanalysis. *Quart. J. Roy. Meteor. Soc.*, **146**, 1999–2049, https://doi.org/10.1002/qj.3803.

Jia, G. J., H. E. Epstein, and D. A. Walker, 2003: Greening of Arctic Alaska, 1981–2001. *Geophys. Res. Lett.*, **30**, 2067, https://doi.org/10.1029/2003GL018268.

Jonasson, S., 1988: Evaluation of the point intercept method for the estimation of plant biomass. *Oikos*, **52**, 101–106, https://doi.org/10.2307/3565988.

Jorgenson, M. T., 2000: Hierarchical organization of ecosystems at multiple spatial scales on the Yukon-Kuskokwim Delta, Alaska, U.S.A. *Arct. Antarct. Alp. Res.*, **32**, 221–239, https://doi.org/10.1080/15230430.2000.12003360.

——, and J. E. Roth, 2010: Landscape classification and mapping for the Yukon-Kuskokwim Delta, Alaska. ABR, Inc.—Environmental Research & Services Doc., 24 pp.

——, G. V. Frost, and D. Dissing, 2018: Drivers of landscape changes in coastal ecosystems on the Yukon-Kuskokwim Delta, Alaska. *Remote Sens.*, **10**, 1280, https://doi.org/10.3390/rs10081280.

Jorgenson, T., and C. Ely, 2001: Topography and flooding of coastal ecosystems on the Yukon-Kuskokwim Delta, Alaska: implications for sea-level rise. *J. Coastal Res.*, **17**, 124–136.

Ju, J., and J. G. Masek, 2016: The vegetation greenness trend in Canada and US Alaska from 1984–2012 Landsat data. *Remote Sens. Environ.*, **176**, 1–16, https://doi.org/10.1016/j.rse.2016.01.001.

Karl, J. W., S. E. McCord, and B. C. Hadley, 2017: A comparison of cover calculation techniques for relating point-intercept vegetation sampling to remote sensing imagery. *Ecol. Indic.*, **73**, 156–165, https://doi.org/10.1016/j.ecolind.2016.09.034.

Kemppinen, J., P. Niittynen, J. Aalto, P. C. le Roux, and M. Luoto, 2019: Water as a resource, stress and disturbance shaping tundra vegetation. *Oikos*, **128**, 811–822, https://doi.org/10.1111/oik.05764.

Kirwan, M. L., G. R. Guntenspergen, A. D'Alpaos, J. T. Morris, S. M. Mudd, and S. Temmerman, 2010: Limits on the adaptability of coastal marshes to rising sea level. *Geophys. Res. Lett.*, **37**, L23401 https://doi.org/10.1029/2010GL045489.

Klein, D. R., 1966: Waterfowl in the economy of the Eskimos on the Yukon-Kuskokwim Delta, Alaska. *Arctic*, **19**, 319–336, https://doi.org/10.14430/arctic3438.

Kokelj, S. V., and Coauthors, 2012: Using multiple sources of knowledge to investigate northern environmental change: Regional ecological impacts of a storm surge in the outer Mackenzie Delta, N.W.T. *Arctic*, **65**, 257–272, https://doi.org/10.14430/arctic4214.

Landrum, L., and M. M. Holland, 2020: Extremes become routine in an emerging new Arctic. *Nat. Climate Change*, **10**, 1108–1115, https://doi.org/10.1038/s41558-020-0892-z.

Lantz, T. C., S. V. Kokelj, and R. H. Fraser, 2015: Ecological recovery in an Arctic delta following widespread saline incursion. *Ecol. Appl.*, **25**, 172–185, https://doi.org/10.1890/14-0239.1.

Latifovic, R., D. Pouliot, and C. Dillabaugh, 2012: Identification and correction of systematic error in NOAA AVHRR long-term satellite data record. *Remote Sens. Environ.*, **127**, 84–97, https://doi.org/10.1016/j.rse.2012.08.032.

Lauzon, R., A. Piliouras, and J. C. Rowland, 2019: Ice and permafrost effects on delta morphology and channel dynamics. *Geophys. Res. Lett.*, **46**, 6574–6582, https://doi.org/10.1029/2019GL082792.

Lawrence, D. M., A. G. Slater, R. A. Tomas, M. M. Holland, and C. Deser, 2008: Accelerated Arctic land warming and permafrost degradation during rapid sea ice loss. *Geophys. Res. Lett.*, **35**, L11506, https://doi.org/10.1029/2008GL033985.

Macander, M. J., 2005: MODIS satellite vegetation indices over partially vegetated pixels on the Arctic coastal plain of Alaska. M.S. thesis, Dept. of Forest Sciences, University of Alaska Fairbanks, 113 pp.

Macias-Fauria, M., B. C. Forbes, P. Zetterberg, and T. Kumpula, 2012: Eurasian Arctic greening reveals teleconnections and the potential for structurally novel ecosystems. *Nat. Climate Change*, **2**, 613–618, https://doi.org/10.1038/nclimate1558.

——, S. R. Karlsen, and B. C. Forbes, 2017: Disentangling the coupling between sea ice and tundra productivity in Svalbard. *Sci. Rep.*, **7**, 8586, https://doi.org/10.1038/s41598-017-06218-8.

Menne, M. J., and Coauthors, 2012: Global Historical Climatology Network–Daily (GHCN–Daily), version 3.26. NOAA/National Climatic Data Center, https://doi.org/10.7289/V5D21VHZ.

Michaelides, R. J., and Coauthors, 2019: Inference of the impact of wildfire on permafrost and active layer thickness in a discontinuous permafrost region using the Remotely Sensed Active Layer Thickness (ReSALT) algorithm. *Environ. Res. Lett.*, **14**, 035007, https://doi.org/10.1088/1748-9326/aaf932.

Miles, V. V., and I. Esau, 2016: Spatial heterogeneity of greening and browning between and within bioclimatic zones in northern west Siberia. *Environ. Res. Lett.*, **11**, 115002, https://doi.org/10.1088/1748-9326/11/11/115002.

Mueter, F. J., and M. A. Litzow, 2008: Sea ice retreat alters the biogeography of the Bering Sea continental shelf. *Ecol. Appl.*, **18**, 309–320, https://doi.org/10.1890/07-0564.1.

Myers-Smith, I. H., and Coauthors, 2011: Shrub expansion in tundra ecosystems: Dynamics, impacts and research priorities. *Environ. Res. Lett.*, **6**, 045509, https://doi.org/10.1088/1748-9326/6/4/045509.

——, and Coauthors, 2020: Complexity revealed in the greening of the Arctic. *Nat. Climate Change*, **10**, 106–117, https://doi.org/10.1038/s41558-019-0688-1.

Myneni, R. B., C. D. Keeling, C. J. Tucker, G. Asrar, and R. R. Nemani, 1997: Increased plant growth in the northern high latitudes from 1981 to 1991. *Nature*, **386**, 698–702, https://doi.org/10.1038/386698a0.

Nitze, I., and G. Grosse, 2016: Detection of landscape dynamics in the Arctic Lena Delta with temporally dense Landsat time-series stacks. *Remote Sens. Environ.*, **181**, 27–41, https://doi.org/10.1016/j.rse.2016.03.038.

Nowacki, G., P. Spencer, M. Fleming, T. Brock, and M. T. Jorgenson, 2003: Ecoregions of Alaska: 2001. USGS Open-File Rep. 2002–29, https://doi.org/10.3133/ofr2002297.

Pachauri, R. K., and Coauthors, 2014: *Climate Change 2014: Synthesis Report.* Cambridge University Press, 151 pp., https://www.ipcc.ch/site/assets/uploads/2018/02/SYR_AR5_FINAL_full.pdf.

Palm, S. P., S. T. Strey, J. Spinhirne, and T. Markus, 2010: Influence of Arctic sea ice extent on polar cloud fraction and vertical structure and implications for regional climate. *J. Geophys. Res.*, **115**, D21209, https://doi.org/10.1029/2010JD013900.

Park, T., and Coauthors, 2016: Changes in growing season duration and productivity of northern vegetation inferred from long-term remote sensing data. *Environ. Res. Lett.*, **11**, 084001, https://doi.org/10.1088/1748-9326/11/8/084001.

Pastick, N. J., M. T. Jorgenson, B. K. Wylie, S. J. Nield, K. D. Johnson, and A. O. Finley, 2015: Distribution of near-surface permafrost in Alaska: Estimates of present and future conditions. *Remote Sens. Environ.*, **168**, 301–315, https://doi.org/10.1016/j.rse.2015.07.019.

——, and Coauthors, 2019: Spatiotemporal remote sensing of ecosystem change and causation across Alaska. *Global Change Biol.*, **25**, 1171–1189, https://doi.org/10.1111/gcb.14279.

Pekel, J. F., A. Cottam, N. Gorelick, and A. S. Belward, 2016: High-resolution mapping of global surface water and its long-term changes. *Nature*, **540**, 418–422, https://doi.org/10.1038/nature20584.

Perry, P., 2010: Unit 18 moose management report. Moose management report of survey and inventory activities 1 July 2007–30 June 2009, P. Harper, Ed., Alaska Department of Fish and Game Management Rep., 271–285, https://www.adfg.alaska.gov/static/home/library/pdfs/wildlife/mgt_rpts/10_moose.pdf.

Piao, S., and Coauthors, 2019: Characteristics, drivers and feedbacks of global greening. *Nat. Rev. Earth Environ.*, **1**, 14–27, https://doi.org/10.1038/s43017-019-0001-x.

Pinzon, J., and C. Tucker, 2014: A non-stationary 1981–2012 AVHRR NDVI3g time series. *Remote Sens.*, **6**, 6929–6960, https://doi.org/10.3390/rs6086929.

Potter, C., and O. Alexander, 2020: Changes in vegetation phenology and productivity in Alaska over the past two decades. *Remote Sens.*, **12**, 1546, https://doi.org/10.3390/rs12101546.

Raynolds, M. K., and D. A. Walker, 2016: Increased wetness confounds Landsat-derived NDVI trends in the central Alaska North Slope region, 1985–2011. *Environ. Res. Lett.*, **11**, 085004, https://doi.org/10.1088/1748-9326/11/8/085004.

——, J. Comiso, D. Walker, and D. Verbyla, 2008: Relationship between satellite-derived land surface temperatures, Arctic vegetation types, and NDVI. *Remote Sens. Environ.*, **112**, 1884–1894, https://doi.org/10.1016/j.rse.2007.09.008.

——, D. A. Walker, H. E. Epstein, J. E. Pinzon, and C. J. Tucker, 2012: A new estimate of tundra-biome phytomass from trans-Arctic field data and AVHRR NDVI. *Remote Sens. Lett.*, **3**, 403–411, https://doi.org/10.1080/01431161.2011.609188.

——, and Coauthors, 2019: A raster version of the Circumpolar Arctic Vegetation Map (CAVM). *Remote Sens. Environ.*, **232**, 111297, https://doi.org/10.1016/j.rse.2019.111297.

Rearden, A., and A. Fienup-Riordan, 2014: *Nunamta Ellamta-llu Ayuqucia: What Our Land and World Are Like*. Calista Elders Council and Alaska Native Language Center, 656 pp.

Reichle, L. M., H. E. Epstein, U. S. Bhatt, M. K. Raynolds, and D. A. Walker, 2018: Spatial heterogeneity of the temporal dynamics of Arctic tundra vegetation. *Geophys. Res. Lett.*, **45**, 9206–9215, https://doi.org/10.1029/2018GL078820.

Roy, D. P., V. Kovalskyy, H. K. Zhang, E. F. Vermote, L. Yan, S. S. Kumar, and A. Egorov, 2016: Characterization of Landsat-7 to Landsat-8 reflective wavelength and normalized difference vegetation index continuity. *Remote Sens. Environ.*, **185**, 57–70, https://doi.org/10.1016/j.rse.2015.12.024.

Santer, B. D., T. M. L. Wigley, J. S. Boyle, D. J. Gaffen, J. J. Hnilo, D. Nychka, D. E. Parker, and K. E. Taylor, 2000: Statistical significance of trends and trend differences in layer-average atmospheric temperature time series. *J. Geophys. Res.*, **105**, 7337–7356, https://doi.org/10.1029/1999JD901105.

Schaaf, C. B., and Z. Wang, 2020: MCD43A4 v006 MODIS/Terra+Aqua Nadir BRDF-Adjusted Reflectance (NBAR) Daily L3 Global 500 m SIN Grid. NASA EOSDIS Land Processes DAAC, https://doi.org/10.5067/MODIS/MCD43A4.006.

Sen, P. K., 1968: Estimates of the regression coefficient based on Kendall's tau. *J. Amer. Stat. Assoc.*, **63**, 1379–1389, https://doi.org/10.1080/01621459.1968.10480934.

Shippert, M. M., D. A. Walker, N. A. Auerbach, and B. E. Lewis, 1995: Biomass and leaf-area index maps derived from SPOT images for Toolik Lake and Imnavait Creek areas, Alaska. *Polar Rec.*, **31**, 147–154, https://doi.org/10.1017/S0032247400013644.

Spencer, D. L., U. C. Nelson, and W. A. Elkins, 1951: America's greatest goose-brant nesting area. *Transactions of the North American Wildlife Conference*, American Wildlife Institute, 290–295.

Taylor, P. C., R. C. Boeke, Y. Li, and D. W. J. Thompson, 2019: Arctic cloud annual cycle biases in climate models. *Atmos. Chem. Phys.*, **19**, 8759–8782, https://doi.org/10.5194/acp-19-8759-2019.

Terenzi, J., M. T. Jorgenson, and C. R. Ely, 2014: Storm-surge flooding on the Yukon-Kuskokwim Delta, Alaska. *Arctic*, **67**, 360–374, https://doi.org/10.14430/arctic4403.

Theil, H., 1992: A rank-invariant method of linear and polynomial regression analysis. *Contributions to Economics and Econometrics*, Springer, 345–381.

Tucker, C. J., and P. J. Sellers, 1986: Satellite remote sensing of primary production. *Int. J. Remote Sens.*, **7**, 1395–1416, https://doi.org/10.1080/01431168608948944.

——, J. H. Elgin, J. E. McMurtrey, and C. J. Fan, 1979: Monitoring corn and soybean crop development with hand-held radiometer spectral data. *Remote Sens. Environ.*, **8**, 237–248, https://doi.org/10.1016/0034-4257(79)90004-X.

——, J. E. Pinzon, M. E. Brown, D. A. Slayback, E. W. Pak, R. Mahoney, E. F. Vermote, and N. E. Saleous, 2005: An extended AVHRR 8-km NDVI dataset compatible with MODIS and SPOT vegetation NDVI data. *Int. J. Remote Sens.*, **26**, 4485–4498, https://doi.org/10.1080/01431160500168686.

Verdonen, M., L. T. Berner, B. C. Forbes, and T. Kumpula, 2020: Periglacial vegetation dynamics in Arctic Russia: Decadal analysis of tundra regeneration on landslides with time series satellite imagery. *Environ. Res. Lett.*, **15**, 105020, https://doi.org/10.1088/1748-9326/abb500.

Vermaire, J. C., M. F. J. Pisaric, J. R. Thienpont, C. J. Courtney Mustaphi, S. V. Kokelj, and J. P. Smol, 2013: Arctic climate warming and sea ice declines lead to increased storm surge activity. *Geophys. Res. Lett.*, **40**, 1386–1390, https://doi.org/10.1002/grl.50191.

Walker, D. A., and Coauthors, 2003: Phytomass, LAI, and NDVI in northern Alaska: Relationships to summer warmth, soil pH, plant functional types, and extrapolation to the circumpolar Arctic. *J. Geophys. Res.*, **108**, 8169, https://doi.org/10.1029/2001JD000986.

White, J. H. R., J. E. Walsh, and R. L. Thoman Jr., 2021: Using Bayesian statistics to detect trends in Alaskan precipitation. *Int. J. Climatol.*, **41**, 2045–2059, https://doi.org/10.1002/joc.6946.

Whitley, M. A., G. V. Frost, M. T. Jorgenson, M. J. Macander, C. V. Maio, and S. G. Winder, 2018: Assessment of LiDAR and spectral techniques for high-resolution mapping of sporadic permafrost on the Yukon-Kuskokwim Delta, Alaska. *Remote Sens.*, **10**, 258, https://doi.org/10.3390/rs10020258.

Xu, L., and Coauthors, 2013: Temperature and vegetation seasonality diminishment over northern lands. *Nat. Climate Change*, **3**, 581–586, https://doi.org/10.1038/nclimate1836.

Ye, W., A. I. J. M. van Dijk, A. Huete, and M. Yebra, 2021: Global trends in vegetation seasonality in the GIMMS NDVI3g and their robustness. *Int. J. Appl. Earth Obs. Geoinf.*, **94**, 102238, https://doi.org/10.1016/j.jag.2020.102238.